

## Relativistic global and local divergences in hydrogenic systems: A study in position and momentum spaces

J. Antolín,<sup>1,2</sup> J. C. Angulo,<sup>3,2,\*</sup> S. Mulas,<sup>3</sup> and S. López-Rosa<sup>4</sup>

<sup>1</sup>*Departamento de Física Aplicada, EINA, Universidad de Zaragoza, 50018-Zaragoza, Spain*

<sup>2</sup>*Instituto Carlos I de Física Teórica y Computacional, Universidad de Granada, 18071-Granada, Spain*

<sup>3</sup>*Departamento de Física Atómica, Molecular y Nuclear, Universidad de Granada, 18071-Granada, Spain*

<sup>4</sup>*Departamento de Física Aplicada II, Escuela Técnica Superior de Ingeniería de Edificación, Universidad de Sevilla, 41012-Sevilla, Spain*

(Received 4 June 2014; published 27 October 2014)

Relativistic effects in one-particle densities of hydrogenic systems are quantified by means of global and local density functionals: the Jensen-Shannon and the Jensen-Fisher divergences, respectively. The Schrödinger and Dirac radial densities are compared, providing complementary results in position and momentum spaces. While the electron cloud gets compressed towards the origin in the Dirac case, the momentum density spreads out over its domain, and the raising of minima in position space does not occur in the momentum space. Regarding the dependence on the nuclear charge and the state quantum numbers for all divergences here considered, as well as their mutual interconnection, accurate powerlike laws  $y \approx Cx^a$  are found systematically. The parameters  $\{C, a\}$  defining the respective dependences are extremely sensitive to the closeness of the system to the ground and/or the circular state. Particularly interesting are the analyses of (i) the plane subtended by the Jensen-Shannon and Jensen-Fisher divergences, in a given space (position or momentum), and (ii) either of the above two divergences in the position-momentum plane. These kinds of results show the complementary role of global and local divergences and that of both conjugate spaces.

DOI: [10.1103/PhysRevA.90.042511](https://doi.org/10.1103/PhysRevA.90.042511)

PACS number(s): 31.30.jz, 31.15.-p, 02.50.Cw, 04.20.Jb

### I. INTRODUCTION

The solutions of the Schrödinger equation for an atomic system with nuclear charge  $Z$  provide a description of the eigenstates in a nonrelativistic framework. In spite of their relevance, it has not been an easy task to determine those solutions, requiring the use of sophisticated models and/or numerical routines. The only exceptions to the above are the one-electron systems, i.e., hydrogenlike atoms. Solutions of both ground and excited states are well known in the aforementioned nonrelativistic framework. Their analytical expressions allow a straightforward determination of the wave functions in the conjugate space, as well as the position and momentum one-particle densities  $\rho(\vec{r})$  and  $\gamma(\vec{p})$ , respectively.

These densities play a relevant role within the so-called “information theory,” allowing an interpretation of many density functionals in terms of physical and chemical properties in many-electron systems. In doing this, a variety of tools and magnitudes have been considered in the literature. Some density functionals deserve special attention, such as the Shannon entropy [1] and the Fisher information [2] among others.

Composite functionals defined, most usually, in terms of (at least) one of the aforementioned Shannon and Fisher quantities, have been studied, both theoretically and numerically, in recent years. They belong to the class of “complexity measures,” enclosing different definitions in order to quantify such a subjective concept as complexity (see Ref. [3] and references therein).

Furthermore, exploring quantitatively the level of similarity or dissimilarity between two different systems in terms of their densities appears nowadays as a very interesting field.

For this aim, different measures of “similarity” [4] and “divergence,” [5,6] have been introduced and, in some cases, later generalized.

The study of the relativistic effects on the just mentioned densities and/or functionals has been the focus of attention of many researchers, not only for hydrogenlike atoms but also for many-electron systems. In order to take into account the relativistic effects, the Dirac-Fock equation must be solved, including the Schrödinger one as the nonrelativistic limit. Solving the Dirac equation is a much more difficult task compared to that for the Schrödinger case. Nevertheless, the aforementioned analytical expressions for the nonrelativistic hydrogenic case are also available for the relativistic position and momentum densities.

Let us mention here some previous works, focused on the analysis of the relativistic effects on the one-particle densities. A pioneering attempt to do this was carried out by studying the charge density  $\rho(\vec{r})$  of hydrogenlike systems in their ground and excited states, in, e.g., Ref. [7], with successful results. In that work no density functionals were considered, but the density itself, in position space. Much more recent are the studies of relativistic effects on density functionals. Among them, the Fisher information for the charge density of neutral atoms [8] and the position- and momentum-space densities of hydrogenlike systems [9], all of them in the ground state, also provide interesting conclusions. Within Ref. [9] many other quantities are considered in both conjugated spaces: the Shannon and Rényi entropies, variance, relative entropy, and López-Ruiz, Mancini, and Calbet [10] (LMC) or shape complexity, all of them only for ground-state hydrogen.

Further studies of complexity measures are also well known within the relativistic framework. Let us mention the analysis of LMC and Shiner-Davison-Landsberg [11] (SDL) complexities in position space for neutral atoms [12], and the comparative study based on LMC and Fisher-Shannon

\*Corresponding author: [angulo@ugr.es](mailto:angulo@ugr.es)

[13] (FS) complexities provided in Ref. [14] for excited hydrogen.

Regarding other comparative measures of recent interest, works on the quantum similarity index (QSI) deserve to be mentioned. Let us note the study of atomic QSI in both position and momentum spaces provided in Ref. [15], where that functional is applied to different systems and/or states separately for the Schrödinger and the Dirac cases. Using the same functional, a direct comparison between the relativistic and nonrelativistic densities for a variety of atoms was provided in a pioneering work [16], by considering the functional dependence on the respective charge densities (i.e., only in position space).

The main aim of this work is to study the relativistic effects on hydrogenic systems with nuclear charge  $Z$  in arbitrary states, by means of their one-particle densities in both position and momentum spaces. For this purpose we compute the so-called “Jensen-Shannon” (JSD) [5,6] and “Jensen-Fisher” (JFD) [17] divergences between the Dirac and Schrödinger densities for a given system and state. The JSD quantifies differences in the overall dispersion of the distributions, while the JFD does the same regarding their gradient content and their relative oscillations.

The paper is structured as follows: In Sec. II, the Jensen-Shannon and Jensen-Fisher divergences are defined for arbitrary probability distributions, emphasizing their meaning as comparative measures within an information-theoretical framework. In Sec. III we describe the distributions considered in this work, namely, relativistic and nonrelativistic hydrogenic densities for arbitrary states, in both position and momentum spaces. Section IV is devoted to the numerical analysis of divergences among the aforementioned densities, paying attention to the functional dependence of the JSD and JFD on the nuclear charge and the state quantum numbers, as well as to the JSD-JFD mutual relationship and uncertaintylike (i.e., position-momentum) interconnections. Conclusions are given in Sec. V, where some open problems are also proposed.

## II. JENSEN-SHANNON AND JENSEN-FISHER DIVERGENCES

Several measures of information for general probability densities [i.e., non-negative functions  $\rho(\vec{r})$  whose integral over their domain obeys the normalization constraint  $\int \rho(\vec{r})d\vec{r} = 1$ ] have been considered in the literature. The most commonly used in information theory is the Shannon entropy  $S$  [1,18],

$$S(\rho) \equiv - \int \rho(\vec{r}) \ln \rho(\vec{r}) d\vec{r}, \quad (1)$$

a global measure of the spread or delocalization of a distribution  $\rho(\vec{r})$ . The definition and applications of the Fisher information  $F$  appear complementary to the functional  $S$  [2]:

$$F(\rho) \equiv \int \rho(\vec{r}) |\vec{\nabla} \ln \rho(\vec{r})|^2 d\vec{r}, \quad (2)$$

a spreading measure of  $\rho(\vec{r})$  with a locality property because it is a functional of its gradient. Contrary to the Shannon entropy, the Fisher information quantifies the pointwise concentration and the gradient content of the distribution, thus revealing

its irregularities and providing a quantitative estimation of its oscillatory character.

Information-theoretic properties based on Shannon entropy and/or Fisher information have been extensively employed in recent years within a quantum-mechanical framework, in particular for multielectronic systems. Their use in atomic and molecular systems has provided a wide variety of results [19–26], including recent studies on complexity measures.

The relative entropy or Kullback and Leibler (KL) divergence [27]

$$D_{\text{KL}}(\rho_1, \rho_2) \equiv \int \rho_1(\vec{r}) \ln \frac{\rho_1(\vec{r})}{\rho_2(\vec{r})} d\vec{r} \quad (3)$$

is the pioneering global measure of differences between probability distributions. It quantifies the information supplied by the data for discriminating between the distributions, being a “directed measure” (therefore not symmetric). Especially remarkable is its property of non-negativity, and the minimum null value is reached only for identical distributions  $\rho_1 = \rho_2$ .

The KL relative entropy constitutes an essential tool within information theory, as shown by its applications for obtaining minimum cross-entropy estimations and for determining atomic [28] and molecular [29] properties, among others. More recent applications include the introduction of an informational quantum dissimilarity measure to study the relativistic effects on the electron density [16], or the employment of KL measures to analyze molecular reaction paths [30].

A closely related information measure between two or more distributions, namely, the Jensen-Shannon divergence,

$$D_{\text{JS}}(\rho_1, \rho_2) \equiv \frac{1}{2} \left[ D_{\text{KL}} \left( \rho_1, \frac{\rho_1 + \rho_2}{2} \right) + D_{\text{KL}} \left( \rho_2, \frac{\rho_1 + \rho_2}{2} \right) \right], \quad (4)$$

was also introduced [5,6]. From its definition, the JSD represents the mean dissimilarity (understood in terms of the KL measure) of each density with respect to their arithmetic mean. Notice the symmetry of the JSD (i.e., the invariance under the exchange of  $\rho_1$  and  $\rho_2$ ), and also that the main properties of the KL divergence are transferred to the JSD: the Jensen-Shannon divergence is always non-negative, vanishing only if  $\rho_1 = \rho_2$ . In fact, the JSD is the square of a true metric [31,32] or, in other words, its square root constitutes a distance in a rigorous mathematical sense.

Using the above definition together with Eqs. (1) and (3), the Jensen-Shannon divergence can also be expressed in terms of the Shannon entropy as

$$D_{\text{JS}}(\rho_1, \rho_2) = S \left( \frac{\rho_1 + \rho_2}{2} \right) - \frac{1}{2} [S(\rho_1) + S(\rho_2)], \quad (5)$$

allowing the JSD divergence to be interpreted also as the “entropy excess” of the mean density with respect to the mean entropy of the individual densities. So we observe that the aforementioned non-negativity of the JSD arises from the convexity of the Shannon entropy functional  $S$ . Different properties and generalizations of the JSD have been discussed and employed in past years [33–38]. This divergence has been widely applied to the analysis and characterization of symbolic sequences or series, and particularly to the study of

segmentation of DNA sequences [39]. However, its use in the framework of quantum information theory [40,41] or in the study of multielectronic systems [42–44] is very recent.

The JSD measure defined above quantifies how similar or different two distributions are over their whole domain, according to its definition in terms of the Shannon entropy. It would also be of great interest to dispose of divergence measures displaying a deeper local character, namely, with values more sensitive to relative strong local changes and/or their respective oscillatory behaviors. As mentioned before, the Fisher information  $F$  given by Eq. (2) possesses this local character.

Because of its meaning as a quantifier of pointwise concentration, the Fisher-like divergence has also been proposed for arbitrary distributions [17,42] and applied to quantum-mechanical systems [42,45]. Recent proposals are inspired on those based on the Shannon entropy. Such is the case of the so-called “Fisher divergence” (FD) and the “Jensen-Fisher divergence” (JFD).

The Fisher divergence is defined in terms of the relative Fisher information  $F_{\text{rel}}$  of  $\rho_1$  with respect to  $\rho_2$  [46]:

$$F_{\text{rel}}(\rho_1, \rho_2) \equiv \int \rho_1(\vec{r}) \left| \vec{\nabla} \ln \frac{\rho_1(\vec{r})}{\rho_2(\vec{r})} \right|^2 d\vec{r}. \quad (6)$$

So  $F_{\text{rel}}$  is a directed measure of relative information as is the KL measure. Its symmetrized version provides the Fisher divergence  $D_{\text{F}}(\rho_1, \rho_2) \equiv F_{\text{rel}}(\rho_1, \rho_2) + F_{\text{rel}}(\rho_2, \rho_1)$  for arbitrary distributions whenever the involved integrals converge. Such is the case of one-particle densities in both position and momentum spaces, for atomic systems in their ground state, with successful applications in recent years for neutral and ionized species [42,43]. Let us notice the non-negativity of both  $F_{\text{rel}}$  and the FD, vanishing only for  $\rho_1 = \rho_2$ .

In Ref. [17], the difficulties of the FD in dealing with pairs of distributions having noncommon zeros were emphasized. Taking into account the definition in Eq. (6), the existence of zeros in  $\rho_1$  and/or  $\rho_2$  causes the integrals in the FD (one at least) to diverge. As described in the next section, a variety of the distributions considered in the present work possess a number of zeros, and therefore the application of the FD is forbidden for them.

The aforementioned difficulties gave rise to a new proposal for a Fisher-like divergence in that work: the Jensen-Fisher divergence [17]. Its definition is inspired by those of the KL and JSD functionals in the Shannon case:

$$D_{\text{JF}}(\rho_1, \rho_2) \equiv \frac{1}{2} \left[ F_{\text{rel}} \left( \rho_1, \frac{\rho_1 + \rho_2}{2} \right) + F_{\text{rel}} \left( \rho_2, \frac{\rho_1 + \rho_2}{2} \right) \right], \quad (7)$$

in a similar fashion as the expression of  $D_{\text{JS}}$  in Eq. (4), replacing  $D_{\text{KL}}$  by  $F_{\text{rel}}$ . Two comments are in order: (i) as for previous comparative measures, the JFD is non-negative and reaches its minimum null value for  $\rho_1 = \rho_2$ , and (ii) working with the previous equation and the definition of  $F_{\text{rel}}$ , an alternative expression for the JFD is achieved:

$$D_{\text{JF}}(\rho_1, \rho_2) = \frac{1}{2} [F(\rho_1) + F(\rho_2)] - F \left( \frac{\rho_1 + \rho_2}{2} \right), \quad (8)$$

in a similar fashion to Eq. (5) by replacing the Shannon functional  $S$  by the Fisher functional  $F$ . Notice the reverse order of the terms leading to the JSD and JFD, Eqs. (5) and (8), respectively, due to the concavity of  $F$  as opposed to the convexity of  $S$ .

### III. HYDROGENIC DIRAC AND SCHRÖDINGER DENSITIES

As mentioned in the Introduction, the main aim of this work is to quantify the relativistic effects in hydrogenic systems. In doing so, we perform a comparative study of the differences between the corresponding relativistic and nonrelativistic densities by computing their Jensen-Shannon and Jensen-Fisher divergences, in both position and momentum spaces.

Previous comparative studies with similar aims to the present one can be classified into three different categories:

(1) Comparisons between the relativistic and nonrelativistic atomic density functions, regarding their shape and structural patterns [7]. These studies provide, most often, qualitative rather than quantitative results. Especially remarkable are the relativistic effects, in position space, of raising the minima and contraction towards the nucleus of the electron density.

(2) Analyses based on the comparison between relevant density functionals of the relativistic and nonrelativistic densities [9,12,14,47,48]. A variety of functionals have been considered: Shannon and Rényi entropies, Fisher information, statistical complexities or complexity ratios, among others. Most usually, the main conclusions of these studies are based on the assumption that a similarity between the values of a given functional for a pair of densities is associated with a similarity between the self densities, which is not necessarily true.

(3) Direct comparisons between distributions by means of a double-density functional, as in the present work. A variety of functionals have been considered in a quantum-mechanical framework, but not so many in order to quantify relativistic effects. Recent applications have been considered for neutral atoms, by means of QSI in position [16,49] and momentum [49] spaces, and also for some special functions of mathematical physics [17] by means of the JSD and JFD.

From the above enumeration, let us remark that (i) studies in momentum space are much more scarce than in the position space, and (ii) all comparative studies for hydrogenic systems (to the best of our knowledge) were carried out by using techniques of the first and second categories above, but not of the third one. This work tries to fill these gaps for hydrogenic systems, regarding applications in momentum space and the employment of divergencelike functionals.

The Dirac wave functions of the stationary states of a hydrogenic system with nuclear charge  $Z$  are described by the eigensolutions  $(E, \Psi_D)$  of the Dirac equation of an electron moving in a Coulomb potential [7,50]. The stationary states are characterized by the quantum numbers  $(n, k, m_j)$ , with the principal quantum number  $n \in \mathbb{N}$ , the Dirac or relativistic quantum number  $k = \pm 1, \pm 2, \dots, -n$ , and  $-j \leq m_j \leq j$  where  $j = \frac{1}{2}, \frac{3}{2}, \dots, n - \frac{1}{2}$  is the total angular momentum number. In addition,  $k = \mp(j + \frac{1}{2})$  for  $j = l \pm \frac{1}{2}$ , so that  $k = -(l + 1)$  if  $j = l + \frac{1}{2}$  and  $k = l$  if  $j = l - \frac{1}{2}$ . Consequently,

for a given  $l \neq 0$  there are the two options  $j = l \pm \frac{1}{2}$ , and conversely (i.e., for a given  $j$ , two values of  $l$  are allowed).

The energy eigenvalues  $E$  are analytically expressed [51–53] in terms of  $n$  and the absolute value  $|k|$ , as well as the term  $\alpha Z$  with  $\alpha = 1/137.035\,999\,11$  the fine-structure constant:

$$E = M \left( 1 + \frac{(\alpha Z)^2}{(n - |k| + \sqrt{k^2 - (\alpha Z)^2})^2} \right)^{-1/2}, \quad (9)$$

where  $M = m_0 c^2$ , with  $m_0$  the rest mass of the electron. The eigenenergies become complex if  $\alpha Z > 1$ , an inequality which imposes the constraint  $Z \leq 137$  for the allowed values of the nuclear charge  $Z$  [54,55].

The Dirac probability density  $\rho_D(\vec{r}) = |\Psi_D(\vec{r})|^2$  for an arbitrary state, using polar coordinates, is separable into a radial factor and an angular one, as

$$\rho_D(\vec{r}) = \rho_D(r)\chi(\theta), \quad (10)$$

with  $\chi(\theta)$  a linear combination of spherical harmonics  $|Y_{l,m_j \pm 1/2}|^2$ ,

$$\chi(\theta) = \langle l, m_j - \frac{1}{2}; \frac{1}{2}, +\frac{1}{2} | j, m_j \rangle^2 |Y_{l, m_j - 1/2}|^2 + \langle l, m_j + \frac{1}{2}; \frac{1}{2}, -\frac{1}{2} | j, m_j \rangle^2 |Y_{l, m_j + 1/2}|^2, \quad (11)$$

and  $\rho_D(r)$  expressed in terms of Kummer confluent hypergeometric functions,

$$\rho_D(r) = |g_{nk}(r)|^2 + |f_{nk}(r)|^2, \quad (12)$$

where  $g$  and  $f$  are the so-called “large” and “small” radial components, respectively (see the Appendix). Normalization to unity of the whole density  $\rho_D(\vec{r})$  translates into the equality  $\int_0^\infty (|g|^2 + |f|^2)r^2 dr = 1$ .

A similar separability of the radial and angular parts holds for the momentum density  $\gamma_D(\vec{p}) = |\tilde{\Psi}_D(\vec{p})|^2$ , with  $\tilde{\Psi}_D(\vec{p})$  being the three-dimensional Fourier transform of  $\Psi_D(\vec{r})$ . The factorization  $\gamma_D(\vec{p}) = \gamma_D(p)\chi(\theta)$  contains the same angular part  $\chi(\theta)$  as in position space [see Eq. (11)], the radial one being

$$\gamma_D(p) = |G_{nk}(p)|^2 + |F_{nk}(p)|^2, \quad (13)$$

with the respective large ( $G$ ) and small ( $F$ ) components, provided in the Appendix, verifying the normalization condition  $\int_0^\infty (|G|^2 + |F|^2)p^2 dp = 1$ .

The nonrelativistic limit of the Dirac radial part, in both conjugated spaces, provides the corresponding ones in the Schrödinger case, keeping the angular part. In fact, the small component tends to zero, so the Schrödinger probability density in position space has the separable expression

$$\rho_S(\vec{r}) = \rho_S(r)\chi(\theta), \quad (14)$$

with  $\rho_S(r)$  determined by the large component, and similarly in momentum space. One of the factors in the Schrödinger radial part is a Laguerre or a Gegenbauer polynomial, in position and momentum spaces, respectively (see the Appendix). Regarding the energy levels, the expression  $E_S = -\hbar^2 Z^2 / 2a_0^2 n^2$  is well known for the nonrelativistic case [56]. The subscript has been added in order to avoid confusion with the Dirac energy  $E$  given by Eq. (9).

For the hydrogenic densities ( $\rho_S, \rho_D$ ) and ( $\gamma_S, \gamma_D$ ) here considered, their factorization into a radial and an angular part, all

sharing the angular one for a given state, produces the angular contribution to cancel out in computing the JSD or JFD. In other words, the dissimilarity between the whole densities arises from that of their respective radial parts, a fact which yields the equalities  $D_{JS}[\rho_S(\vec{r}), \rho_D(\vec{r})] = D_{JS}[\rho_S(r), \rho_D(r)]$  and  $D_{JS}[\gamma_S(\vec{p}), \gamma_D(\vec{p})] = D_{JS}[\gamma_S(p), \gamma_D(p)]$ , and similarly for  $D_{JF}$ .

The scaling properties of the Schrödinger eigenfunctions with the nuclear charge  $Z$ , in both conjugate spaces, are well known. They allow the radial density  $\rho_S(Z; r)$  to be straightforwardly obtained for a system with nuclear charge  $Z$  in a given state from that of the system with  $Z = 1$  in the same state, namely, from  $\rho_S(1; r)$ , and similarly in momentum space. For the Schrödinger one-particle densities of three-dimensional hydrogen, these properties read

$$\rho_S(Z; r) = Z^3 \rho_S(1; Zr) \quad \text{and} \quad \gamma_S(Z; p) = Z^{-3} \gamma_S(1; p/Z). \quad (15)$$

The properties in Eq. (15) for  $\rho_S$  and  $\gamma_S$  translate into the following regarding the dependences of the Shannon and Fisher functionals on the nuclear charge  $Z$ :

$$S[\rho_S(Z; r)] = S[\rho_S(1; r)] - 3 \ln Z, \quad (16)$$

$$F[\rho_S(Z; r)] = Z^2 F[\rho_S(1; r)],$$

$$S[\gamma_S(Z; p)] = S[\gamma_S(1; p)] + 3 \ln Z, \quad (17)$$

$$F[\gamma_S(Z; p)] = Z^{-2} F[\gamma_S(1; p)].$$

The question now is the following: does  $\rho_D(Z; r)$  verify the same scaling property as  $\rho_S(Z; r)$ , given by Eq. (15)? Of course, the same question is pertinent regarding  $\gamma_S(Z; p)$ . Before providing an answer, let us analyze the implications of assuming that the above equalities are valid for both the Schrödinger and the Dirac densities, and for their arithmetic mean as well:

(a) Neither  $D_{JS}(\rho_S, \rho_D)$  nor  $D_{JS}(\gamma_S, \gamma_D)$  would depend on the nuclear charge  $Z$  (this is a consequence of the cancellation of the term  $3 \ln Z$  when computing the JSD from the three Shannon terms).

(b)  $D_{JF}(\rho_S, \rho_D)$  would be proportional to the square  $Z^2$  of the nuclear charge, and to  $Z^{-2}$  in momentum space (these are consequences of the same proportionalities for the three Fisher terms appearing in the JFD).

However, this is not the case, because Eq. (15) is not verified in the Dirac case, as will be discussed in Sec. IV D.

#### IV. QUANTIFYING RELATIVISTIC EFFECTS: NUMERICAL ANALYSIS OF HYDROGENIC DIVERGENCES

It is well known that the relativistic effects are more apparent when dealing with heavier quantum systems. Such is the case, for instance, of the hydrogenic cations with large nuclear charge  $Z$ . Most studies on relativistic effects in one-electron atoms have dealt with the energy spectra, various expectation values, and the structural properties of the charge density. Among the last, it is worthmaking the following observations after comparing the relativistic density

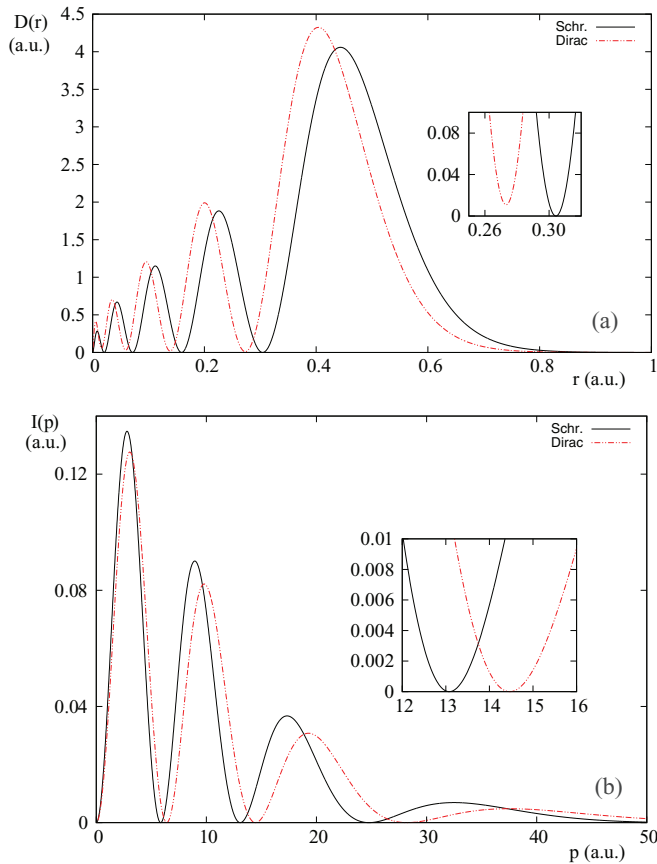


FIG. 1. (Color online) Schrödinger and Dirac radial densities in (a) position space,  $D(r) = r^2 \rho(r)$ , and (b) momentum space,  $I(p) = p^2 \gamma(p)$ , for the state  $(n = 5, l = 0, j = 1/2)$  of  $\text{Th}^{89+}$  (nuclear charge  $Z = 90$ ). Atomic units (a.u.) are used.

profiles with the nonrelativistic ones [7]: (i) contraction of the radial density profile  $D(r) = r^2 \rho(r)$  towards the origin, and (ii) raising of the minima, i.e., the nonrelativistic radial density vanishes at their local minima, but the corresponding values of the relativistic density are nonzero. Both effects are clearly displayed in Fig. 1(a) for  $Z = 90$  (hydrogenic thorium,  $\text{Th}^{89+}$ ) in the state characterized by the quantum numbers  $n = 5, l = 0$ , and  $j = 1/2$ .

These are the main qualitative descriptions of relativistic effects on the charge density of the systems here considered, recently analyzed in a quantitative way by means of the so-called complexity ratios [14]. However, it appears pertinent to ask ourselves about the relevance of relativistic effects in the conjugated space or, in other words, on the momentum-space radial density profile  $I(p) = p^2 \gamma(p)$ . Considering the well-known uncertainty principle [57], one would expect that a contraction (i.e., a higher localization) in one space has to be accompanied by a spreading in the complementary space. The function  $I(p)$  is displayed in Fig. 1(b) for the aforementioned system and state, in both the relativistic (Dirac) and nonrelativistic (Schrödinger) cases. Some comments are in order: (i) as expected, the relativistic density spreads out compared with the nonrelativistic one, and (ii) in contrast to the nodes in position space, the nonrelativistic ones in momentum space are not raised, but are only shifted.

Considering Schrödinger-Dirac divergences as measures of dissimilarity between the relativistic and nonrelativistic distributions, one should expect a monotonically increasing behavior of the divergence as long as the nuclear charge  $Z$  increases. For many-electron systems, other features such as, e.g., the shell-filling patterns, could also be relevant in the JSD and JFD as functions of  $Z$ , but this is not the case for the one-electron systems here considered.

Let us denote as  $D_{\text{JS}}^r(\text{Sch,Dir})$  and  $D_{\text{JF}}^r(\text{Sch,Dir})$  the Jensen-Shannon and Jensen-Fisher divergences, respectively, between the Schrödinger (i.e., nonrelativistic) and Dirac (i.e., relativistic) position-space densities ( $\rho_S$  and  $\rho_D$ , respectively) for a given system with nuclear charge  $Z$  and the quantum numbers  $(n, l, j, m_j)$  specifying its state. A similar notation will be employed for the momentum-space distributions  $\gamma_S$  and  $\gamma_D$ , within the framework just mentioned, by using the superscript  $p$ . Let us notice that  $m_j$  appears only in the angular part of the density and, consequently, the only quantum numbers to be considered in order to determine the JSD and JFD are  $(n, l, j)$ .

It is worth remembering the relationships between the orbital ( $l$ ) and total ( $j$ ) quantum numbers, namely,  $j = l \pm 1/2$  and  $l = j \mp 1/2$  as long as both are non-negative. Corresponding with these (in general) one-to-two interconnections, notations such as  $(n, l, \pm)$  will also be considered. For illustration,  $(3, 1, +)$  stands for the state with  $(n = 3, l = 1, j = 3/2)$ . For fixed  $n$  we have a number of  $(n, l, j)$  states given by  $2n - 1$ , because of the  $n$  allowed values  $l = 0, \dots, n - 1$ , and, for each one with the only exception  $l = 0$ , there are two compatible values of  $j$ . Relevant particular cases correspond to  $(n, 0, +)$  and  $(n, n - 1, +)$ , known as  $s$  states and circular states, respectively. Regarding circular states, let us notice that (i) their characterization requires the additional condition  $|m_j| = j$ , irrelevant for the present study on the basis of the radial parts, and (ii) the just mentioned radial parts are nodeless. In fact (see the Appendix) they contain a grade- $(n - |k|)$  polynomial factor, so the absence of nodes arises from the condition  $n = |k|$  holding for circular states.

In spite of the availability of analytical expressions for all the densities we are dealing with (somewhat simple as determined by their polynomial, rational, and/or exponential factors), the same does not hold for their respective JSD and JFD. These difficulties involve the dependence on both the nuclear charge and the state quantum numbers.

In this section we determine numerically the aforementioned JSD and JFD values for a variety of nuclear charges, as well as by considering different quantum states. The numerical results are analyzed, in order to get insight into how the JSD and/or JFD is modified by varying the just mentioned variables, as well as into a possible relationship between the two functionals. We consider that the analysis in both position and momentum spaces is completely justified, having in mind previous studies on many-electron systems by means of the JSD, JFD, and other comparative functionals [42,45,49].

Usually, systems with nuclear charges within the range  $Z = 1-100$  will be considered throughout. The only exception to the comment above is the quantity  $D_{\text{JF}}^p$  (i.e., the Jensen-Fisher divergence in momentum space), computed for  $Z = 10-100$ . The reason for disregarding the lowest values  $Z =$

TABLE I. Parameters and correlation coefficients of the linear regressions for position-space Jensen-Shannon ( $D_{\text{JS}}^r$ ) and Jensen-Fisher ( $D_{\text{JF}}^r$ ) divergences with a functional dependence  $CZ^a$  on the nuclear charge  $Z \leq 100$  of hydrogenic systems in the states  $(n, l, j)$ .

State	Position space					
	Power $a$	Jensen-Shannon $D_{\text{JS}}^r$ Coefficient $C$	Correlation	Power $a$	Jensen-Fisher $D_{\text{JF}}^r$ Coefficient $C$	Correlation
(4,0,+)	3.95	$9.2 \times 10^{-10}$	0.99993	3.56	$5.3 \times 10^{-5}$	0.997
(4,1,-)	3.98	$8.1 \times 10^{-10}$	0.99998	3.76	$1.7 \times 10^{-5}$	0.997
(4,1,+)	3.84	$1.9 \times 10^{-10}$	0.9998	3.30	$3.7 \times 10^{-5}$	0.998
(4,2,-)	3.93	$1.3 \times 10^{-10}$	0.99994	3.46	$9.1 \times 10^{-6}$	0.997
(4,2,+)	3.77	$4.8 \times 10^{-11}$	0.9996	3.15	$1.7 \times 10^{-5}$	0.9994
(4,3,-)	4.01	$1.3 \times 10^{-11}$	0.9999993	5.98	$1.5 \times 10^{-12}$	0.999998
(4,3,+)	4.01	$2.6 \times 10^{-12}$	0.9999992	6.01	$1.9 \times 10^{-13}$	0.9999993
(3,0,+)	3.91	$9.4 \times 10^{-10}$	0.9998	3.47	$1.1 \times 10^{-4}$	0.997
(3,1,-)	3.98	$7.0 \times 10^{-10}$	0.99993	3.72	$2.2 \times 10^{-5}$	0.996
(3,1,+)	3.75	$1.7 \times 10^{-10}$	0.9995	3.19	$6.0 \times 10^{-5}$	0.9991
(3,2,-)	4.01	$5.0 \times 10^{-11}$	0.99997	5.84	$3.2 \times 10^{-11}$	0.99996
(3,2,+)	4.01	$5.9 \times 10^{-12}$	0.999998	6.02	$1.1 \times 10^{-12}$	0.999998
(2,0,+)	3.80	$1.1 \times 10^{-9}$	0.9992	3.34	$3.0 \times 10^{-4}$	0.997
(2,1,-)	4.04	$4.0 \times 10^{-10}$	0.99991	5.02	$4.0 \times 10^{-8}$	0.9998
(2,1,+)	4.02	$1.9 \times 10^{-11}$	0.99999	6.04	$1.4 \times 10^{-11}$	0.99999
(1,0,+)	4.11	$1.1 \times 10^{-10}$	0.9997	6.17	$9.7 \times 10^{-10}$	0.9998

1–9 is the appearance of numerical instabilities in computing  $D_{\text{JF}}^p$  (Sch,Dir), as given by Eq. (8). For those very light systems, relativistic effects are less relevant and, consequently, zeros of both  $\gamma_S$  and  $\gamma_D$  as well as those of the arithmetic mean  $(\gamma_S + \gamma_D)/2$  are extremely close. At those locations, the integrands of the three terms appearing in Eq. (8) possess an almost identical finite limit, so cancellations of terms provide extremely low values, at times below the numerical accuracy of the integration procedures. This problem does not appear in computing either  $D_{\text{JS}}$  (because of the absence of quotients in the integrands) or  $D_{\text{JF}}^p$  [because of the elevation of the minima in  $\rho_D$  and, consequently, in the arithmetic mean  $(\rho_S + \rho_D)/2$  also].

#### A. Dependence on the nuclear charge

In order to grasp the dependence of the Schrödinger-Dirac divergence on the nuclear charge  $Z$ , let us analyze the results for a variety of quantum states, in both position and momentum spaces.

(1) Ground state  $(1,0,+)$ . All divergences (i.e., the JSD and JFD, in  $r$  and  $p$  spaces) for the ground state are observed to depend on the nuclear charge  $Z$  in a similar fashion, namely, as  $CZ^a$ . Regarding the values of the parameters  $C$  and  $a$  (see Tables I and II), some comments are in order:

(a) Linear regressions provide the functional dependences  $D_{\text{JS}}^r \approx C^r Z^{4.11}$  and  $D_{\text{JS}}^p \approx C^p Z^{3.99}$ , with the respective correlation coefficients 0.99974 and 0.99997, and multiplicative constants  $C^r = 1.1 \times 10^{-10}$  and  $C^p = 4.0 \times 10^{-10}$ .

(b) The momentum space  $D_{\text{JS}}^p$  is larger than  $D_{\text{JS}}^r$  for any  $Z$ , as highlighted by the value of the quotient  $C^p/C^r \approx 3.6$ . This value, together with the above-mentioned functional dependence of the corresponding divergences on  $Z$ , causes their quotient to be in the interval  $D_{\text{JS}}^p/D_{\text{JS}}^r \in [2.1, 3.6]$  for any  $Z = 1-100$ . The reason for obtaining such different numbers in the  $r$  and  $p$  spaces is the structural features of

the respective radial density profiles  $D(r)$  and  $I(p)$ . For the ground state, both functions are unimodal, with the absolute maximum located, in the nonrelativistic case, at  $r_{\text{max}} = 1/Z$  and  $p_{\text{max}} = Z/\sqrt{3}$  (in atomic units, a.u.): for a medium-heavy system, say  $Z = 50$ , the above locations are  $r_{\text{max}} = 0.02$  and  $p_{\text{max}} = 28.87$ . The main differences between Schrödinger and Dirac densities occur around their absolute maxima, within an extremely narrow interval in position space, much wider in the momentum one. For illustration, the Schrödinger and Dirac  $D(r)$  display values above one-half of their global height within the interval  $r \in [0.007, 0.042]$  (width 0.035 a.u.), and the same occurs for  $I(p)$  within (roughly)  $p \in [14, 54]$  (width 40 a.u.). With these comments in mind, we grasp now why the ground-state  $D_{\text{JS}}^p$  displays higher values than  $D_{\text{JS}}^r$  for a given system.

(c) The corresponding data for the JFD are the following:  $D_{\text{JF}}^r \approx C^r Z^{6.17}$  and  $D_{\text{JF}}^p \approx C^p Z^{1.95}$ , with correlation coefficients 0.9998 and 0.99996, respectively, and multiplicative constants  $C^r = 9.7 \times 10^{-10}$  and  $C^p = 2.0 \times 10^{-9}$ . Now it happens that much larger values of the JFD are found in position space, as compared to the corresponding ones in momentum space. For illustration,  $D_{\text{JF}}^r/D_{\text{JF}}^p \approx 10^4$  ( $Z = 11$ ),  $10^6$  ( $Z = 32$ ),  $10^8$  ( $Z = 94$ ).

Let us notice that the previous JFD quotient increases as quickly as  $Z^{4.22}$ , in contrast to  $D_{\text{JS}}^r/D_{\text{JS}}^p \approx 0.275Z^{0.12}$ , only slightly sensitive to the value of the nuclear charge  $Z$ . For arbitrary  $Z$  we find  $D_{\text{JS}}^p \geq 2.092D_{\text{JS}}^r$ , while  $D_{\text{JF}}^p \leq 2.062D_{\text{JF}}^r$ . The illustrative values above for the JFD position-momentum quotient transform into the following for the JSD case:  $D_{\text{JS}}^r/D_{\text{JS}}^p \approx 0.37$  ( $Z = 11$ ),  $0.42$  ( $Z = 32$ ),  $0.47$  ( $Z = 94$ ).

(2) Excited states in position space. Let us now consider the simplest wave functions beyond the ground state, namely, those with values  $n = 2, 3, \dots$  of the principal quantum number. From the analysis of Figs. 2(a) ( $D_{\text{JS}}^r$ ) and 2(b) ( $D_{\text{JF}}^r$ ), drawn by using a double-logarithmic scale, some comments are in order:

TABLE II. Parameters and correlation coefficients of the linear regressions for momentum-space Jensen-Shannon ( $D_{JS}^p$ ) and Jensen-Fisher ( $D_{JF}^p$ ) divergences with a functional dependence  $CZ^a$  on the nuclear charge  $Z \leq 100$  of hydrogenic systems in the states  $(n, l, j)$ .

Momentum space						
State	Power $a$	Jensen-Shannon $D_{JS}^p$		Power $a$	Jensen-Fisher $D_{JF}^p$	
		Coefficient $C$	Correlation		Coefficient $C$	Correlation
(4,0,+)	4.00	$7.5 \times 10^{-10}$	0.99998	0.015	$5.3 \times 10^{-2}$	0.95
(4,1,-)	4.00	$7.3 \times 10^{-10}$	0.99999	0.011	$3.2 \times 10^{-2}$	0.93
(4,1,+)	3.99	$1.1 \times 10^{-10}$	0.99998	-0.002	$1.3 \times 10^{-2}$	0.72
(4,2,-)	4.00	$9.0 \times 10^{-11}$	0.99998	0.003	$4.7 \times 10^{-3}$	0.91
(4,2,+)	4.00	$2.1 \times 10^{-11}$	0.99999	0.003	$2.3 \times 10^{-3}$	0.89
(4,3,-)	4.01	$1.2 \times 10^{-11}$	0.999998	1.99	$3.6 \times 10^{-9}$	0.999997
(4,3,+)	4.00	$3.3 \times 10^{-12}$	0.9999995	2.00	$9.7 \times 10^{-10}$	0.999998
(3,0,+)	4.01	$6.4 \times 10^{-10}$	0.99999	0.006	$1.4 \times 10^{-2}$	0.89
(3,1,-)	4.02	$5.7 \times 10^{-10}$	0.99998	0.023	$4.8 \times 10^{-3}$	0.94
(3,1,+)	4.00	$7.1 \times 10^{-11}$	0.999993	0.009	$1.7 \times 10^{-3}$	0.90
(3,2,-)	4.02	$4.1 \times 10^{-11}$	0.999993	1.99	$5.7 \times 10^{-9}$	0.999998
(3,2,+)	4.01	$8.3 \times 10^{-12}$	0.999999	2.00	$1.1 \times 10^{-9}$	0.9999995
(2,0,+)	4.02	$4.8 \times 10^{-10}$	0.99998	0.046	$1.1 \times 10^{-3}$	0.92
(2,1,-)	4.08	$3.0 \times 10^{-10}$	0.9999	2.00	$1.5 \times 10^{-8}$	0.999999
(2,1,+)	4.01	$3.2 \times 10^{-11}$	0.999997	1.99	$1.3 \times 10^{-9}$	0.999996
(1,0,+)	3.99	$4.0 \times 10^{-10}$	0.99997	1.95	$2.0 \times 10^{-9}$	0.99996

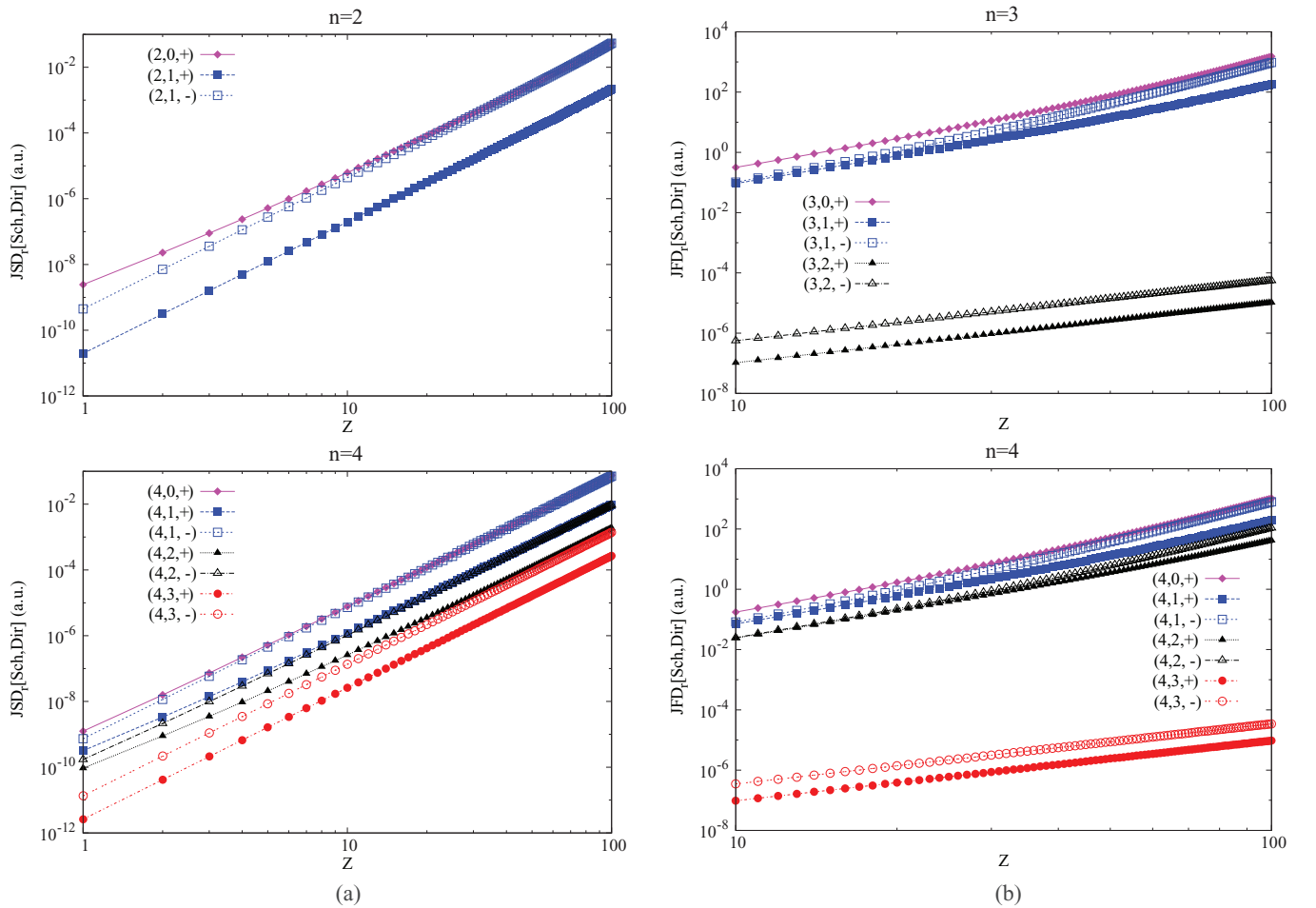


FIG. 2. (Color online) Position-space divergences (a)  $D_{JS}^r$ , and (b)  $D_{JF}^r$  between Schrödinger and Dirac hydrogenic systems with nuclear charge  $Z \leq 100$  for two different values of the principal quantum number  $n$  (top and bottom). Full and empty symbols correspond, respectively, to  $j = l + 1/2$  and  $j = l - 1/2$ . Atomic units (a.u.) are used.

(a) All curves display an extremely linear shape. Such linearity, together with the logarithmic scales employed, translates (as previously observed for the ground state) into a functional dependence

$$D_{\text{JS}}^r \approx CZ^a, \quad (18)$$

and similarly for  $D_{\text{JF}}^r$ . The above parameters are determined by the coefficients of the straight line, estimated from a linear regression. The estimated parameters and the correlation coefficients are provided in Table I. Let us remark the following:

(i) We must distinguish two disjoint intervals for the correlation coefficients of  $\ln D_{\text{JF}}^r$  versus  $\ln Z$ : while all those for  $l = n - 1$  are above 0.9998, they are below 0.9994 if  $l < n - 1$ . These higher or lower linear behaviors are clearly displayed in Fig. 2(b) through the presence of regions of curvature for high  $Z$  in all curves except for those with  $l = n - 1$ . So linearity increases as long as the states approach the circular one. This occurs also for  $D_{\text{JS}}^r$ , but deviations from linearity are very slight in all curves: all correlation coefficients of  $D_{\text{JS}}^r$  for  $n = 1-4$ , with arbitrary  $l$ , are above the aforementioned threshold 0.9994 [the unique exception is the state (2,0,+), with 0.992].

(ii) All powers of  $Z$ , in the  $D_{\text{JS}}^r$  case, are in the narrow interval [3.75,4.11]: usually the functional dependence  $D_{\text{JS}}^r \sim Z^4$  constitutes an accurate approximation.

(iii) The comment above does not hold in the  $D_{\text{JF}}^r$  case. We distinguish two different intervals: [3.15,3.76] for  $l = 0, \dots, n - 2$ , and [5.84,6.17] for  $l = n - 1$ , with the only exception  $a = 5.02$  for the state (2,1,-). The respective accurate approximations are  $D_{\text{JF}}^r \sim Z^{3.5}$  and  $D_{\text{JF}}^r \sim Z^6$ , as well as  $D_{\text{JF}}^r \sim Z^5$  for the aforementioned exception.

(iv) For fixed  $l \geq 1$ , the power of  $Z$  decreases or remains constant in going from  $j = l - 1/2$  to  $j = l + 1/2$ , with the systematic exception  $l = n - 1$  in the  $D_{\text{JF}}^r$  case. For any value of  $n$ , the state displaying the highest optimal power is always the circular one. This comment holds for both  $D_{\text{JS}}^r$  (excepting  $n = 2$ ) and  $D_{\text{JF}}^r$ .

(v) Splitting of curves, as determined by the factor  $C$  in Eq. (18), is more apparent for  $D_{\text{JF}}^r$  than for  $D_{\text{JS}}^r$ : while the differences between the values of  $D_{\text{JS}}^r$  for  $s$  and circular states are of 2–3 orders of magnitude, those of  $D_{\text{JF}}^r$  differ by 7–9 orders of magnitude.

(vi) Summarizing,  $D_{\text{JF}}^r$  displays a higher capability than  $D_{\text{JS}}^r$  to (i) distinguish the behaviors for different states, and (ii) distinguish, in a more remarkable way, the states with  $l = n - 1 > 0$  (which include the circular one) from the whole set of states compatible with a given  $n > 1$ .

(b) For low enough  $Z$ , the position-space  $D_{\text{JS}}^r$  curves can be distinguished from each other as characterized by the quantum numbers determining the corresponding states. Systematic patterns to be emphasized are as follows: (i) for each of the cases  $j = l \pm 1/2$ , the  $D_{\text{JS}}^r$  divergences decrease for increasing  $l$ , (ii) for fixed  $l$ , divergences for  $j = l - 1/2$  are above the corresponding ones for  $j = l + 1/2$ , and (iii) for the whole set of quantum numbers for a given  $n$ , curves are ordered from above to below according to the following criteria: divergences diminish as  $j$  increases and then, once  $j$  is fixed, they diminish for increasing  $l$ . This ordering can be observed more clearly over the vertical axis in the left-hand side.

(c) For high enough  $Z$ , the above criterion regarding the dependence of  $D_{\text{JS}}^r$  on  $j$  remains. However, curves for different  $l$  but identical  $j$  become indistinguishable. This means that, for a given value of the principal quantum number  $n$ , the initial  $2n - 1$  curves in the low- $Z$  region intermingle among themselves as  $Z$  increases, giving rise to a final number of (roughly)  $n$  curves in the high- $Z$  region, as observed over the vertical axis in the right-hand side.

(d) The above behaviors regarding distinguishability of  $D_{\text{JS}}^r$  curves are the opposite for the  $D_{\text{JF}}^r$  curves: the “initially” (i.e., for lowest  $Z$ ) indistinguishable curves  $j = l \pm 1/2$  with identical  $l < n - 1$  are split off for large enough  $Z$ .

(3) Excited states in momentum space. Most of the above comments on  $D_{\text{JS}}^r$  apply also to the Jensen-Shannon divergence  $D_{\text{JS}}^p$  in momentum space [see Fig. 3(a) and Table II], as well as the pertinent ones to the ground state (1,0,+) in both conjugated spaces (see Tables I and II):

(a) The linearity is, on average, higher than in position space. Now, all correlation coefficients are above 0.9999 for  $n = 1-4$ . The maximum linear correlation is always attached to the circular state.

(b) Powers of  $Z$  are within [3.99,4.08], so the estimated dependence  $D_{\text{JS}}^p \sim Z^4$  is slightly more accurate than that of  $D_{\text{JS}}^r$ .

(c) Trends for fixed  $l$  or  $j$  are identical to those in position space, including ordering and mixing of curves for high  $Z$ .

The numerical analysis of the momentum-space Jensen-Fisher divergence  $D_{\text{JF}}^p$  provides a variety of results, most of them very different from those of (i) the corresponding position-space functional  $D_{\text{JF}}^r$ , and (ii) the Jensen-Shannon divergence  $D_{\text{JS}}^p$  in momentum space. The most apparent features and patterns, as displayed in Fig. 3(b) and Table II, are described below:

(a) Curves for noncircular states  $l = 0, 1, \dots, n - 2$  appear only slightly dependent on the nuclear charge  $Z$ , i.e., roughly constant [see Fig. 2(b)]. This fact is emphasized by the values of the parameters given in Table II, obtained from the corresponding linear regressions. For those states, (i) most correlation coefficients range from 0.89 to 0.95, being not so high as for previously discussed functionals, and (ii) the exponent of the powerlike dependence  $Z^a$  is in the interval  $a \in [-0.002, 0.046]$ . These values, so close to the null value, justify the aforementioned roughly constant behavior.

(b) Once again, states with  $l = n - 1$  (enclosing the circular one) behave in a completely different manner. Increase of the  $D_{\text{JF}}^p$  divergence with the nuclear charge  $Z$  is very apparent in Fig. 3(b), for both cases  $n = 3$  and  $n = 4$ . A more detailed dependence on  $Z$  is obtained from the data in Table II. It is first observed that extremely high correlation coefficients are regained, with an accurate functional dependence  $D_{\text{JF}}^p \sim Z^2$  in most cases (the estimated powers range from 1.99 to 2.00, with the only exception 1.95 for the ground state).

(c) The ordering of curves follows the same patterns as for previously discussed functionals, but in a much clearer way: (i) for fixed  $n$ , curves are ordered from above to below as the quantum number  $l$  increases from  $l = 0$  to  $l = n - 1$ , and (ii) for arbitrary  $n$  and  $l \neq 0$ , the curve for the state  $(n, l, -)$  is systematically above its partner  $(n, l, +)$ .

(d) Regarding the multiplicative constant  $C$ , two comments are in order: (i) it is much higher for  $D_{\text{JF}}^p$  than for  $D_{\text{JS}}^p$ , so

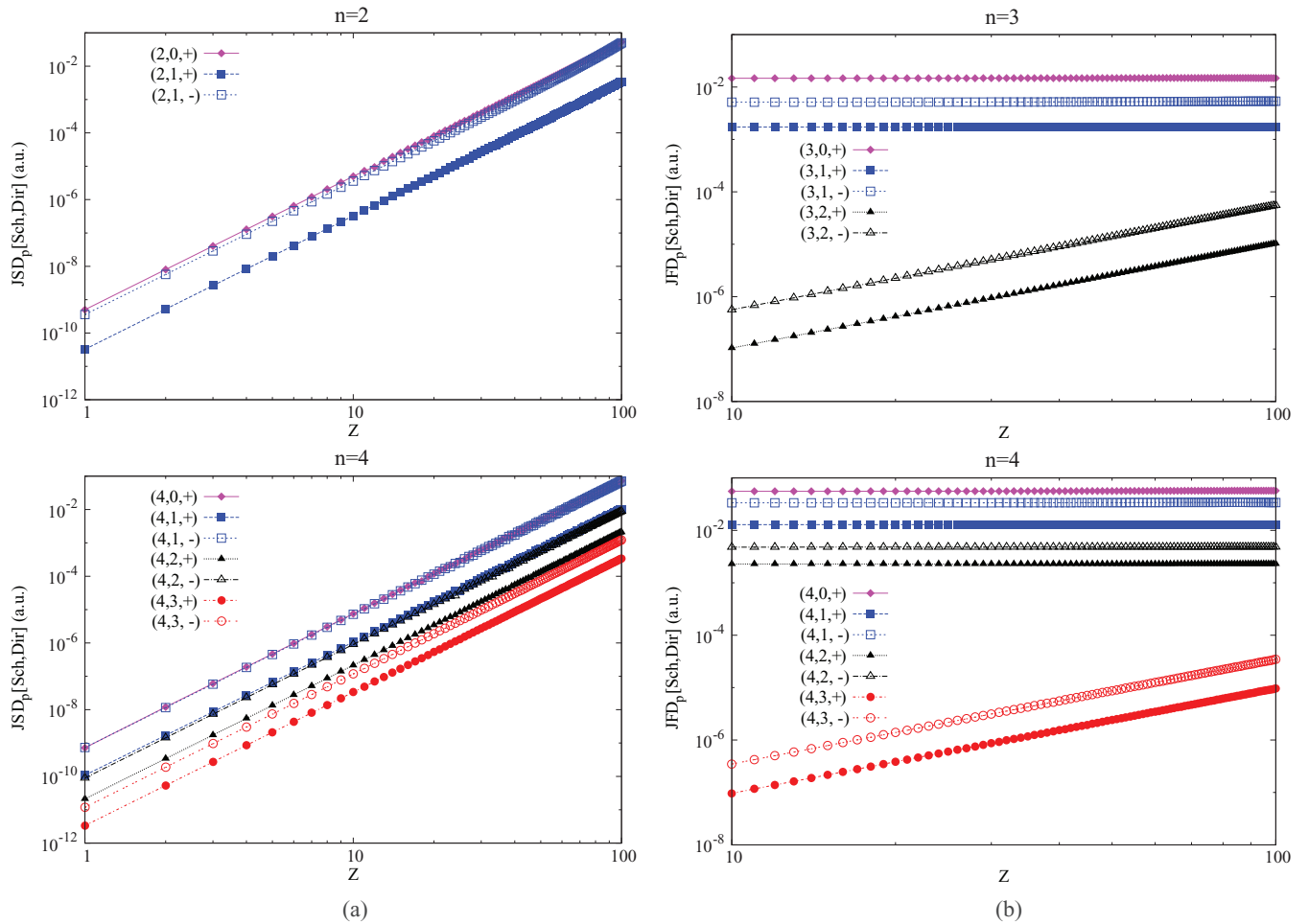


FIG. 3. (Color online) Momentum-space divergences (a)  $D_{\text{JS}}^p$ , and (b)  $D_{\text{JF}}^p$  between Schrödinger and Dirac hydrogenic systems with nuclear charge  $Z \leq 100$  and principal quantum number  $n = 2$  (top) and  $n = 4$  (bottom). Full and empty symbols correspond, respectively, to  $j = l + 1/2$  and  $j = l - 1/2$ . Atomic units (a.u.) are used.

relativistic effects are more apparent at the local level than at the global one in momentum space, and (ii) the “soft” decreasing trend of  $C$  in the  $D_{\text{JS}}^p$  case, as long as  $l$  increases for fixed  $n$ , remains in the  $D_{\text{JF}}^p$  case with the exception of a dramatic fall for  $l = n - 1$ . The last fact will be discussed in more detail in the next section.

So, in spite of the higher rate of increase of  $D_{\text{JS}}^p$  with the nuclear charge  $Z$ , as compared to that of  $D_{\text{JF}}^p$ , the values of the latter for any state are above those of the former. This fact highlights, once again, the relevance of relativistic effects at a local level in momentum space.

### B. Dependence on the quantum numbers

The above patterns regarding the dependence of the divergences on the quantum numbers for fixed  $Z$  are observed more clearly in Fig. 4. In that figure, each of the  $r$  and  $p$  divergences considered in this work is displayed for a unique system (thorium with  $Z = 90$ , for illustration) as a function of the quantum number  $l$ . This is done by means of different curves within the range  $3 \leq n \leq 6$ , each one characterized by a pair of values  $(n, j)$ , constrained by the relationships

$n \geq l + 1$  and  $j = l \pm 1/2$ . Similar comments to those given below apply also for arbitrary  $Z$ .

All curves display a monotonically decreasing behavior, corroborating previous comments on the ordering of divergences depending on the value of  $l$ . However, remarkable differences between the behaviors of the JSD and JFD in position or momentum space appear:

(a) While the decreasing rate of JSD is augmented “softly” up to  $l = n - 1$ , the same occurs for the JFD only up to  $l = n - 2$ . Changes in the JFD values are dramatic for the last step, that is, in passing from  $l = n - 2$  to the boundary value  $l = n - 1$ , and most notably for the circular state. Systematically, in fact, the decrease in going from  $l$  to  $l + 1$  is higher in the  $j = l + 1/2$  case than in the  $j = l - 1/2$  case.

(b) The figures at the top ( $D_{\text{JS}}^p$  and  $D_{\text{JF}}^p$ ) are almost identical in the shape and ordering of curves, as well as in their range of absolute values (observe the numbers throughout the y axis of each figure).

(c) The comment above does not apply at all to the figures at the bottom ( $D_{\text{JF}}^r$  and  $D_{\text{JF}}^p$ ): (i) the JFD curves in Fig. 4(b) appear perfectly ordered and they do not intermingle among themselves, in contrast with the behavior of the position-space curves as displayed in Fig. 4(a), and (ii) the ranges of the

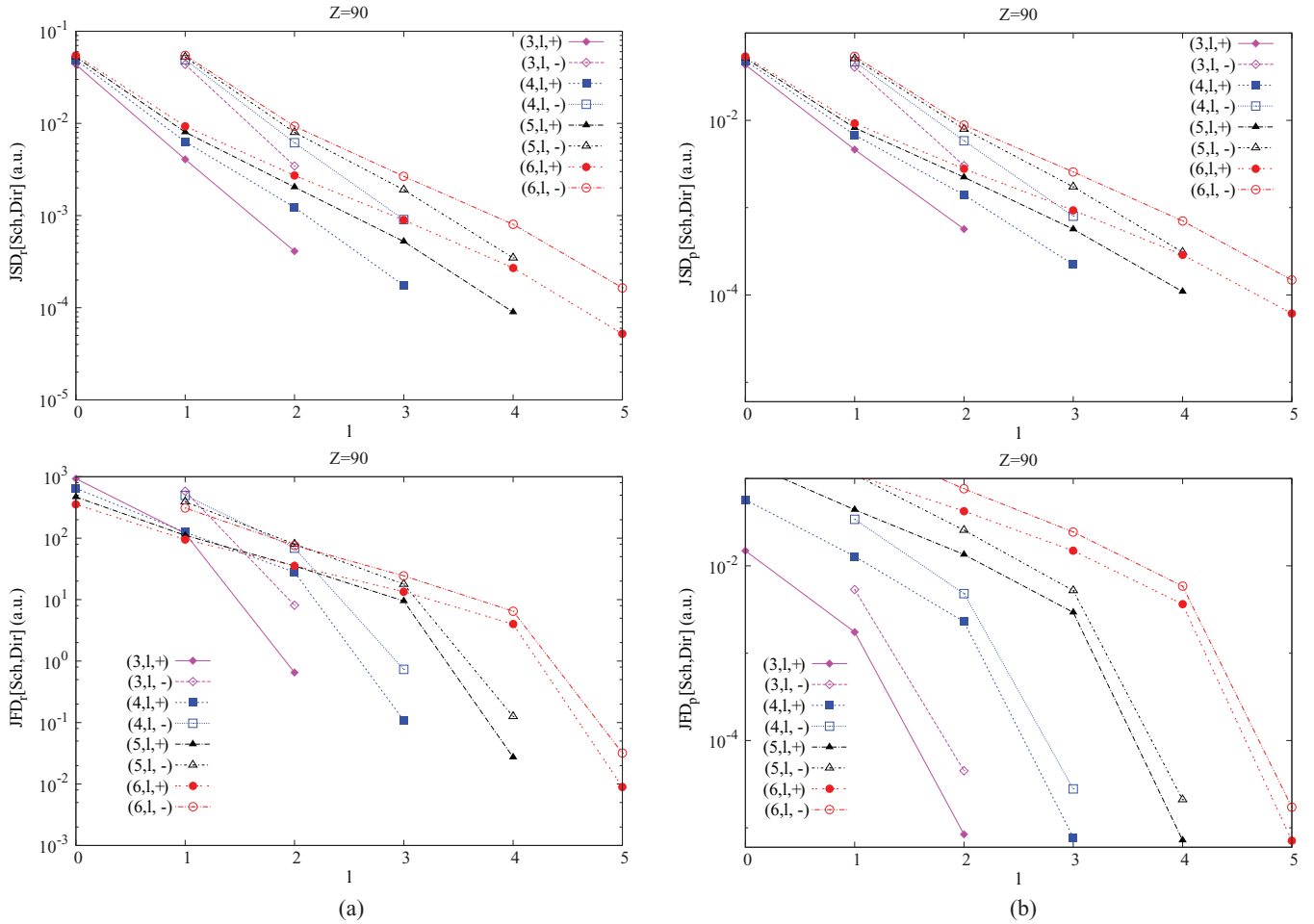


FIG. 4. (Color online) Jensen-Shannon (top) and Jensen-Fisher (bottom) divergences between Schrödinger and Dirac hydrogenic densities of  $\text{Th}^{89+}$  (nuclear charge  $Z = 90$ ) as functions of the orbital quantum number  $l$  for a variety of compatible pairs  $(n, j)$ , in (a) position and (b) momentum spaces. Full and empty symbols correspond, respectively, to  $j = l + 1/2$  and  $j = l - 1/2$ . Atomic units (a.u.) are used.

JFD absolute values are extremely different in position and momentum spaces; the scales of the y axes differ by three orders of magnitude, and for any state of the hydrogenic system  $Z = 90$  here considered, the Schrödinger-Dirac Jensen-Fisher divergence in position space is (roughly)  $10^3$ – $10^5$  times that in momentum space. So the relativistic contraction effect is much more clearly revealed by measuring differences in the content of the gradient of the charge density, as compared to the corresponding measure regarding the spreading effect on the momentum density.

(d) The just mentioned position-momentum JFD ratios are much higher for low values of the principal quantum number  $n$ , and conversely. For illustration, focusing on the  $D_{\text{JF}}^p$  curves for  $n = 3$  [Fig. 4(b), bottom] it is observed that they are located below the rest of the curves. However, in passing to position space [Fig. 4(a), bottom] the corresponding curves are seen to be above many others excepting the extreme point  $l = n - 1$ .

From the analysis of Fig. 4, some additional comments regarding the dependence on the principal quantum number  $n$  are in order. In doing so, let us focus on any fixed  $l$  in the lower shaft, in order to analyze the location of the symbols above that value. For each of the cases  $j = l \pm 1/2$ , the divergence decreases as  $n$  decreases, in accordance with the previous

observation of minimal divergences for states with maximal  $l$ . Again, the decrease of divergence is significant for  $n = l + 1$  (enclosing the circular state), but not so much for higher  $n$  values.

### C. Interrelation between Jensen-like divergences

We wonder now about an eventual interrelation between the JSD and JFD measures, i.e., about a possible functional dependence of one divergence on the other. In order to check the above assumption, Fig. 5 displays the “divergence planes,” subtended by the JSD on one axis and the JFD on the other. This is done in both conjugate spaces, namely, position [Fig. 5(a)] and momentum [Fig. 5(b)]. In doing so, the numerical pairs (JSD,JFD) have been considered for three different systems ( $Z = 1, 20, 100$  in position space;  $Z = 10, 20, 100$  in momentum space) and, for each one, the whole set of states compatible with the value  $n = 6$ .

The main comments arising from the analysis of Fig. 5(a) (position space) are as follows:

(a) As one would expect, heavier systems display higher Schrödinger-Dirac divergences, at both global and local levels. This fact is revealed by the location of symbols for  $Z = 100$

close to the upper right corner. Location at (roughly) the bottom and left halves occurs for a system as light as  $Z = 1$ , while an intermediate situation is found for the medium-light value  $Z = 20$ .

(b) Systematically, the states  $l = n - 1$  suffer a clear shift to the left as compared to their partners with

$$D_{\text{JS}}^r \approx \begin{cases} 1.4 \times 10^{-3} (D_{\text{FD}}^r)^{0.668} & \text{if } l = n - 1 \quad (\text{correlation coefficient } 0.9998), \\ 6.7 \times 10^{-5} (D_{\text{FD}}^r)^{1.173} & \text{if } l < n - 1 \quad (\text{correlation coefficient } 0.9973). \end{cases} \quad (19)$$

This means that increasing  $D_{\text{JF}}^r$  causes  $D_{\text{JS}}^r$  to increase also, but much more along the line with  $l < n - 1$  than along the line with  $l = n - 1$ .

Some of the above comments apply also in momentum space [Fig. 5(b)], namely, higher divergences for heavier systems, and shifts to the left (very clear) and to the bottom (slight) for states with  $l = n - 1$ . However, there appear remarkable differences with respect to the position-space features. The most apparent one is the absence of the two previous ‘‘correlation lines.’’ It is observed that a not so accurate

identical  $Z$ , and also to the bottom but not so apparently.

(c) States with  $l = n - 1$ , on one hand, and  $l < n - 1$  on the other, belong roughly to independent straight lines, the first one above the other and with a lower slope. Linear regressions provide the following functional dependences:

linear correlation (coefficient 0.994) remains for the  $l = n - 1$  states, whose representative points are located in the left half of the plane. But the unique alignment in position space for the rest of the states is now split off in momentum space, depending on the specific  $Z$  value under consideration. A variety of parallel lines are displayed (all them in the right half of the plane), so that the functional dependence

$$D_{\text{JS}}^p \approx C^p(Z) [D_{\text{JF}}^p]^a \quad (20)$$

is found (correlation coefficients 0.983 to 0.985), similar to the interconnection in position space given by Eq. (19). The difference is that the multiplicative parameter  $C^p(Z)$  does not remain constant for arbitrary states and nuclear charges  $Z$ , but increases for increasing  $Z$ . This is not the case of the power  $a$ , which is roughly constant (1.12 to 1.15) for arbitrary systems and states.

In Fig. 6, uncertaintylike relationships are numerically searched for, in both the Jensen-Shannon [Fig. 6(a)] and Jensen-Fisher [Fig. 6(b)] cases. A first comparative look at these figures reveals strong differences between the divergence uncertainty patterns in the JSD and JFD frameworks.

Regarding the JSD, it is clearly observed [Fig. 6(a)] that the position and momentum divergences display similar values, that is,  $D_{\text{JS}}^r \approx D_{\text{JS}}^p$ . A clear exception is displayed, corresponding to the ground state  $n = 1$ , in which the momentum divergence is much higher than the position one; in fact,  $D_{\text{JS}}^p \approx 2D_{\text{JS}}^r$ . We have not yet been able to justify this result from a theoretical basis. The Jensen-Fisher uncertainty plane [Fig. 6(b)] displays extremely different features, as compared to that for the JSD. Now it is worth noting differences in the slopes of the lines for states  $l = n - 1$  with respect to the roughly null ones for the rest of the states. So while the JSD uncertainty plane has more capability to distinguish the ground state from the excited ones, the capability of the JFD uncertainty plane concerns differences between circular and noncircular states. For the circular ones, the functional dependence  $D_{\text{JF}}^p \sim (D_{\text{JF}}^r)^{1/3}$  has been determined numerically.

#### D. Analysis of scaling transformations

Let us recall the conclusions at the end of Sec. III regarding the behavior of the Schrödinger-Dirac JSD and JFD, assuming that the scaling properties given by Eq. (15) hold in both the relativistic and nonrelativistic cases:

(a) The position- and momentum-space JSDs do not depend on the nuclear charge  $Z$ . Or, in other words, all exponents of

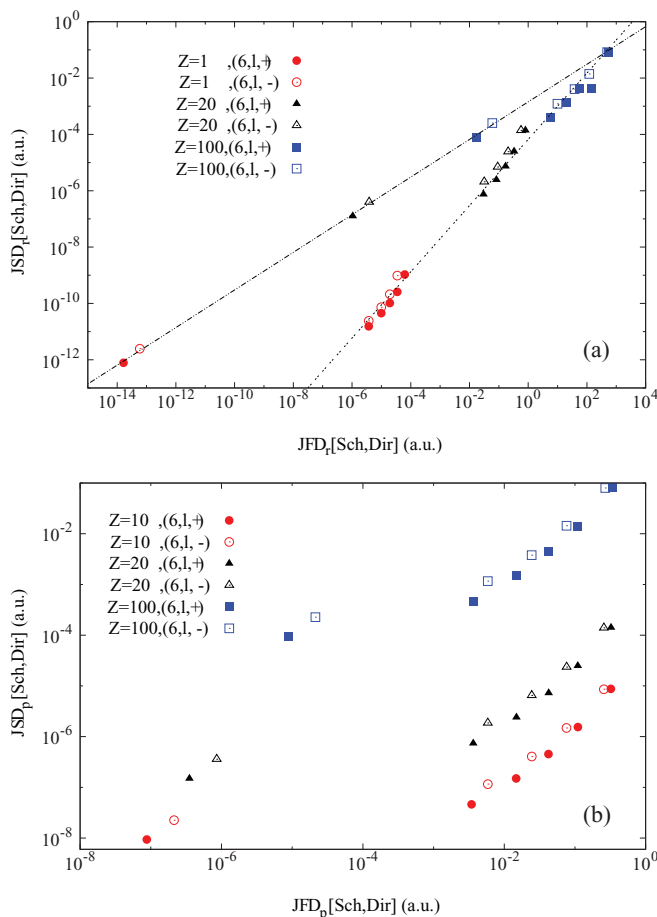


FIG. 5. (Color online) Divergence planes  $D_{\text{JF}}-D_{\text{JS}}$  for all states with principal quantum number  $n = 6$  of systems with three different values of the nuclear charge  $Z$ , in (a) position and (b) momentum spaces. Full and empty symbols correspond, respectively, to  $j = l + 1/2$  and  $j = l - 1/2$ . Atomic units (a.u.) are used.

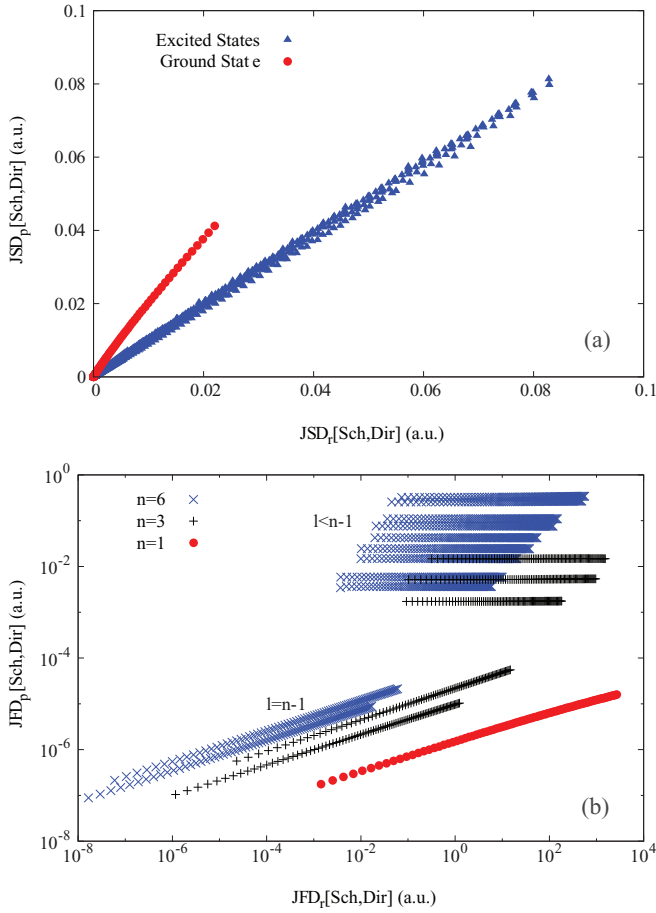


FIG. 6. (Color online) Position-momentum planes (a) Jensen-Shannon  $D'_{JS}-D''_{JS}$ , and (b)  $D'_{JF}-D''_{JF}$  for hydrogenic states with principal quantum numbers  $n = 1-6$  and nuclear charges  $Z \leq 100$ . Atomic units (a.u.) are used.

$Z$  in the JSD columns of Tables I and II should be expected to be exactly zero.

(b) The position-space JFD is proportional to the square  $Z^2$  of the nuclear charge, and the momentum-space JFD to  $Z^{-2}$ . Or, in other words, all exponents of  $Z$  in the JFD column of Tables I and II should be expected to be exactly  $+2$  and  $-2$ , respectively.

In all the above cases, the correlation coefficients should be exactly 1.

It is clear that all these conclusions are clearly in contrast with our numerical results. Why? Because the assumption that  $\rho_D$  and  $\gamma_D$  verify the same scaling properties as do  $\rho_S$  and  $\gamma_S$  is wrong. Let us see this.

For simplicity, let us consider the position-space ground state (with  $n = 1$  and  $k = -1$ ), and only the component  $g(Z; r)$ . The comments below apply similarly to the component  $f(Z; r)$ , and to the components  $F$  and  $G$  in momentum space, also.

If  $\rho_D$  is to verify Eq. (15), both the large and small components should verify

$$\frac{g(Z; r)}{g(1; Zr)} = Z^{3/2}. \quad (21)$$

However, the functions in the quotient read

$$g(Z; r) = 2(\lambda Z)^{3/2} \sqrt{\frac{1 + \gamma_Z}{\Gamma(2\gamma_Z + 1)}} (2\lambda Zr)^{\gamma_Z - 1} e^{-\lambda Zr} \quad (22)$$

and

$$g(1; Zr) = 2\lambda^{3/2} \sqrt{\frac{1 + \gamma_1}{\Gamma(2\gamma_1 + 1)}} (2\lambda Zr)^{\gamma_1 - 1} e^{-\lambda Zr}, \quad (23)$$

with  $\lambda$  defined in the Appendix, and  $\gamma_Z$  denoting the parameter  $\gamma = \sqrt{1 - (\alpha Z)^2}$ , also in the Appendix, but with an explicit subscript here, denoting the value of the nuclear charge considered.

It is clear that, when computing the aforementioned quotient, the explicit dependence on  $Z$  provides the desired result. But an extra dependence on  $Z$  appears, via the parameter  $\gamma_Z$ . So the condition in Eq. (15) would be verified only if  $\gamma_Z = \gamma_1$ , corresponding to the trivial case  $Z = 1$ . Thus the reason for obtaining our numerical results arises from the fact that the scaling properties of the nonrelativistic densities are not verified by the Dirac densities.

## V. CONCLUSIONS AND OPEN PROBLEMS

It is not an easy task to check whether or not two densities share some specific properties by exploring only their plots, and it is even more difficult to quantify the extent to which they do it. Concepts such as, e.g., “differences at global and local levels” are usually unnoticed when comparing the respective curves.

An alternative to the usual comparative procedures based on density plots, Jensen-like divergence measures of global and local character, have been employed in this work. These functionals have allowed the importance of relativistic effects for the one-particle densities of hydrogenic atoms to be quantified, in both position and momentum spaces.

It is worth remarking that using comparative double-density functionals (such as the JSD and JFD) provides a more useful technique for the purposes of our paper, compared to the analysis of functionals of a single density (say  $C$ ), but applied independently for each of the relativistic (Dir) and nonrelativistic (Sch) densities. In this regard, it should be noted that the equality  $C(\text{Sch}) = C(\text{Dir})$  does not guarantee that the densities are identical. However, if either of the JSD or JFD vanishes, we can affirm the equality of the two densities (almost everywhere, at least).

The main conclusions arising from the analysis carried out in the present work are summarized as follows:

(a) The comparative studies in the two conjugated spaces for the JSD and JFD functionals provide very different results. The Jensen-Shannon divergence behaves similarly in both spaces, regarding the dependences on the nuclear charge for arbitrary states and on the angular quantum number for a given system. This comment applies to the qualitative behavior and to the quantitative behavior as well for excited states. This is not the case of the ground state, with higher JSD values in momentum than in position space. Some of these results are explained by considering structural features of the radial densities, such as, e.g., unimodality and location of maxima to justify the ground-state results.

(b) On the contrary, the Jensen-Fisher divergence behaves in different ways within each of the conjugated spaces. In the momentum space, the JFD remains roughly constant for noncircular states when the nuclear charge is varied, but increases monotonically in the circular case.

(c) A variety of relationships have been obtained for both the JSD and JFD in position and/or momentum spaces. In particular, the uncertainty planes subtended by any of these functionals in position and momentum spaces display clearly the above-mentioned comments regarding differences between ground and excited states in the JSD case, and between circular and noncircular states in the JFD case.

The numerical study here described has given rise to a variety of open problems, to be considered in future works. Some of them are worthy of remark:

(a) All four divergence measures considered in this work (i.e., Shannon and Fisher measures in both conjugated spaces) display, for arbitrary states, an extremely accurate powerlike dependence on the nuclear charge of the systems considered. This fact arises from numerical observations, but justification on a theoretical basis is still to be found.

(b) The previous comment applies to the justification of the capability of the global measure to discern the ground state and the local measure to discern circular states.

(c) Further features of the numerical results here discussed deserve to be justified on a theoretical basis (e.g., ordering of the curves  $j = l \pm 1/2$ , dependence on the quantum number  $l$  for fixed  $n$ , and conversely deviation from linearity for noncircular states, splitting and mixing of curves for low or large  $Z$ , etc.).

Previous results dealt with (i) ground-state hydrogenic [9] or many-electron [8,12,15] systems, (ii) position-space measures with no reference to momentum-space ones [8,12], or (iii) single-density functionals instead of double-density ones [8,9,12,14]. The results found in this study highlight the interest of quantifying relativistic effects by measures of divergence, taking into account local and global functionals simultaneously, and both conjugated spaces too.

#### ACKNOWLEDGMENTS

We thank P. A. Bouvrie for his kind help with the relativistic numerical codes. This work was partially supported by the Excellence Projects FQM-4643 and FQM-7276 of the Junta de Andalucía (Spain, EU), and Grant No. FIS2011-24540 of the Ministerio de Innovación y Ciencia. We also acknowledge support from the Andalusian research groups FQM-020 (J.A. and J.C.A.), and FQM-239 (S.L.R.).

#### APPENDIX: EXPLICIT EXPRESSIONS OF DIRAC AND SCHRÖDINGER RADIAL PARTS

In the equations below,  $a_0$  denotes the Bohr radius.

(a) The Schrödinger radial part in position space [56] is

$$\rho_S(r) = \frac{\Gamma(n-l)}{2n\Gamma(n+l+1)} \left(\frac{2Z}{a_0n}\right)^{2l+3} e^{-(2Z/a_0n)r} r^{2l} \times \left[ L_{n-l-1}^{(2l+1)}\left(\frac{2Z}{a_0n}r\right) \right]^2 \quad (\text{A1})$$

with  $L_{n-l-1}^{(2l+1)}$  a Laguerre polynomial.

(b) The Schrödinger radial part in momentum space [56] is

$$\gamma_S(p) = \frac{2^{2l+1}n^4\Gamma^2(l+1)\Gamma(n-l)}{\pi\Gamma(n+l+1)(Zm_0c)^3} \times (1-x)^l(1+x)^{l+4} \left[ C_{n-l-1}^{(l+1)}(x) \right]^2, \quad (\text{A2})$$

with  $x \equiv [Z^2 - n^2(p/m_0c)^2]/[Z^2 + n^2(p/m_0c)^2]$ , and  $C_{n-l-1}^{(l+1)}$  a Gegenbauer polynomial.

(c) The Dirac radial part in position space [7] is  $\rho_D(r) = |g_{nk}(r)|^2 + |f_{nk}(r)|^2$ , with

$$\left. \begin{aligned} g_{nk}(r) \\ f_{nk}(r) \end{aligned} \right\} = \frac{\pm(2\lambda)^{3/2}}{\Gamma(2\gamma+1)} \sqrt{\frac{(M \pm E)\Gamma(2\gamma+n'+1)}{4M \frac{(n'+\gamma)M}{E} \left(\frac{(n'+\gamma)M}{E} - k\right) n!}} (2\lambda r)^{\gamma-1} \times e^{-\lambda r} \left[ \left( \frac{(n'+\gamma)M}{E} - k \right) F(-n', 2\gamma+1; 2\lambda r) \mp n' F(1-n', 2\gamma+1; 2\lambda r) \right] \quad (\text{A3})$$

where  $n' = n - |k| = 0, 1, 2, \dots$  (the radial quantum number),  $\gamma = \sqrt{k^2 - (\alpha Z)^2}$ ,  $\lambda = \frac{1}{\hbar c}(M^2 - E^2)^{1/2}$ , and  $F(a, b; z)$  denotes the Kummer confluent hypergeometric function.

(d) The Dirac radial part in momentum space [58] is  $\gamma_D(p) = |G_{nk}(p)|^2 + |F_{nk}(p)|^2$ , with

$$\begin{aligned} G_{nk}(p) &= i^l \frac{\sqrt{(1+\epsilon)\Gamma(2\gamma+n'+1)/[n'!N(N-k)]}}{4\lambda^{3/2}\Gamma(2\gamma+1)} \\ &\quad \times [n' H(n'-1, 2\gamma+1, \gamma-1, l, p/\lambda) \\ &\quad - (N-k) H(n', 2\gamma+1, \gamma-1, l, p/\lambda)], \quad (\text{A4}) \\ F_{nk}(p) &= i^l \frac{\sqrt{(1-\epsilon)\Gamma(2\gamma+n'+1)/[n'!N(N-k)]}}{4\lambda^{3/2}\Gamma(2\gamma+1)} \\ &\quad \times [n' H(n'-1, 2\gamma+1, \gamma-1, l+1, p/\lambda) \\ &\quad + (N-k) H(n', 2\gamma+1, \gamma-1, l+1, p/\lambda)], \quad (\text{A5}) \end{aligned}$$

where  $\epsilon = E/(m_0c^2)$ ,  $N = (n'+\gamma)/\epsilon$ , and

$$\begin{aligned} H(v, \beta, \delta, l, \sigma) &= \frac{v!\Gamma(\beta)}{\Gamma(l+\frac{3}{2})} 2^{\delta-l+2} \sigma^l \sum_{m=0}^v \frac{(-2)^m \Gamma(m+l+\delta+3)}{m!\Gamma(v-m+1)\Gamma(\beta+m)} \\ &\quad \times {}_2F_1\left(\frac{m+l+\delta+3}{2}, \frac{m+l+\delta+4}{2}, l+\frac{3}{2}; -\sigma^2\right), \quad (\text{A6}) \end{aligned}$$

with  ${}_2F_1$  the Gauss hypergeometric function. This results in an expression which is not in the form of a terminating series, but it can be transformed appropriately into a terminating one [59].

- [1] C. E. Shannon and W. Weaver, *The Mathematical Theory of Communication* (University of Illinois Press, Urbana, 1949).
- [2] R. A. Fisher, *Proc. Cambridge Philos. Soc.* **22**, 700 (1925).
- [3] *Statistical Complexity: Applications in Electronic Structure*, edited by K. D. Sen (Springer, London, 2011).
- [4] R. Carbó-Dorca, J. Arnau, and L. Leyda, *Int. J. Quantum Chem.* **17**, 1185 (1980).
- [5] A. K. C. Wong and M. You, *IEEE Trans. Pattern Anal. Mach. Intell.* **PAMI-7**, 599 (1985).
- [6] C. Rao and T. Nayak, *IEEE Trans. Inf. Theory* **31**, 589 (1985).
- [7] V. M. Burke and I. P. Grant, *Proc. Phys. Soc., London* **90**, 297 (1967).
- [8] A. Borgoo, P. Geerlings, and K. D. Sen, *Phys. Lett. A* **372**, 5106 (2008).
- [9] J. Katriel and K. D. Sen, *J. Comput. Appl. Math.* **233**, 1399 (2010).
- [10] R. López-Ruiz, H. L. Mancini, and X. Calbet, *Phys. Lett. A* **209**, 321 (1995).
- [11] J. S. Shiner, M. Davison, and P. T. Landsberg, *Phys. Rev. E* **59**, 1459 (1999).
- [12] A. Borgoo, F. De Proft, P. Geerlings, and K. D. Sen, *Chem. Phys. Lett.* **444**, 186 (2007).
- [13] K. D. Sen, J. Antolín, and J. C. Angulo, *Phys. Rev. A* **76**, 032502 (2007).
- [14] P. A. Bouvrie, S. López-Rosa, and J. S. Dehesa, *Phys. Rev. A* **86**, 012507 (2012).
- [15] P. Maldonado, A. Sarsa, E. Buendía, and F. J. Gálvez, *Phys. Lett. A* **375**, 2544 (2011).
- [16] A. Borgoo, M. Godefroid, P. Indelicato, F. de Proft, and P. Geerlings, *J. Chem. Phys.* **126**, 044102 (2007).
- [17] P. Sánchez-Moreno, A. Zarzo, and J. S. Dehesa, *J. Phys. A* **45**, 125305 (2012).
- [18] E. T. Jaynes, *Phys. Rev.* **106**, 620 (1957).
- [19] S. B. Sears and S. R. Gadre, *J. Chem. Phys.* **75**, 4626 (1981).
- [20] T. Koga and M. Morita, *J. Chem. Phys.* **79**, 1933 (1983).
- [21] J. C. Angulo, *Phys. Rev. A* **50**, 311 (1994).
- [22] A. N. Tripathi, V. H. Smith, Jr., R. P. Sagar, and R. O. Esquivel, *Phys. Rev. A* **54**, 1877 (1996).
- [23] S. Liu, *J. Chem. Phys.* **126**, 191107 (2007).
- [24] K. Ch. Chatzisavvas, Ch. C. Moustakidis, and C. P. Panos, *J. Chem. Phys.* **123**, 174111 (2005).
- [25] J. C. Angulo and J. Antolín, *J. Chem. Phys.* **128**, 164109 (2008).
- [26] J. C. Angulo, J. Antolín, and K. D. Sen, *Phys. Lett. A* **372**, 670 (2008).
- [27] S. Kullback and A. Leibler, *Ann. Math. Stat.* **22**, 79 (1951).
- [28] J. Antolín, J. C. Cuchi, and J. C. Angulo, *J. Phys. B* **32**, 577 (1999).
- [29] M. Ho, R. P. Sagar, H. Schmider, D. F. Weaver, and V. H. Smith, Jr., *Int. J. Quantum Chem.* **53**, 627 (1995).
- [30] A. Borgoo, P. Jaque, A. Toro-Labbé, C. van Alsenoy, and P. Geerlings, *Phys. Chem. Chem. Phys.* **11**, 476 (2009).
- [31] D. M. Endres and J. E. Schindelin, *IEEE Trans. Inf. Theory* **49**, 1858 (2003).
- [32] F. Österreicher and I. Vajda, *Ann. Inst. Stat. Math* **55**, 639 (2003).
- [33] J. Lin, *IEEE Trans. Inf. Theory* **37**, 145 (1991).
- [34] I. J. Taneja, L. Pardo, D. Morales, and M. L. Menéndez, *Qüestiió (Spain)* **13**, 47 (1989).
- [35] I. J. Taneja, in *Advances in Electronics and Electron Physics* Vol. 76, edited by P. W. Hawkes (Academic Press, New York, 1989), pp. 327–413.
- [36] J. Lin and S. K. M. Wong, *Int. J. Gen. Syst.* **17**, 73 (1990).
- [37] F. Topsoe, *IEEE Trans. Inf. Theory* **46**, 1602 (2000).
- [38] P. W. Lamberti and A. P. Majtey, *Physica A* **329**, 81 (2003).
- [39] P. Bernaola-Galván, I. Grosse, P. Carpena, J. L. Oliver, R. Román-Roldán, and H. E. Stanley, *Phys. Rev. Lett.* **85**, 1342 (2000).
- [40] P. W. Lamberti, A. P. Majtey, A. Borrás, M. Casas, and A. Plastino, *Phys. Rev. A* **77**, 052311 (2008).
- [41] A. P. Majtey, P. W. Lamberti, and D. P. Prato, *Phys. Rev. A* **72**, 052310 (2005).
- [42] J. Antolín, J. C. Angulo, and S. López-Rosa, *J. Chem. Phys.* **130**, 074110 (2009).
- [43] S. López-Rosa, J. Antolín, J. C. Angulo, and R. O. Esquivel, *Phys. Rev. A* **80**, 012505 (2009).
- [44] J. C. Angulo, J. Antolín, S. López-Rosa, and R. O. Esquivel, *Physica A* **389**, 899 (2010).
- [45] A. L. Martín, J. C. Angulo, and J. Antolín, *Physica A* **392**, 5552 (2013).
- [46] P. Hammad, *Rev. Stat. Appl.* **26**, 73 (1978).
- [47] J. Sañudo and R. López-Ruiz, *Phys. Lett. A* **373**, 2549 (2009).
- [48] P. Maldonado, A. Sarsa, E. Buendía, and F. J. Gálvez, *Phys. Lett. A* **374**, 3847 (2010).
- [49] J. C. Angulo and J. Antolín, *J. Chem. Phys.* **126**, 044106 (2007).
- [50] I. P. Grant, *Relativistic Quantum Theory of Atoms and Molecules: Theory and Computation* (Springer, Berlin, 2007).
- [51] W. Greiner, *Relativistic Quantum Mechanics: Wave Equations*, 3rd ed. (Springer, Berlin, 2000).
- [52] G. W. F. Drake, *Handbook of Atomic, Molecular and Optical Physics* (AIP, New York, 1996), pp. 120–134.
- [53] R. A. Swainson and G. W. F. Drake, *J. Phys. A* **24**, 79 (1995).
- [54] O. Klein, *Z. Phys.* **37**, 895 (1929).
- [55] C. Calogeracos and N. Dombey, *Contemp. Phys.* **40**, 313 (1999).
- [56] H. A. Bethe and E. E. Salpeter, *Quantum Mechanics of One- and Two-Electron Systems* (Plenum, New York, 1977).
- [57] W. Heisenberg, *Z. Phys.* **43**, 172 (1927).
- [58] A. Rubinowicz, *Phys. Rev.* **73**, 1330 (1948).
- [59] C. V. Sheth, *Phys. Rev. A* **30**, 1537 (1984).